Hyporheic flow path response to hydraulic jumps at river steps: Hydrostatic model simulations

T. Endreny,[1] L. Lautz,[2] and D. Siegel[2]

Received 17 September 2010; revised 19 November 2010; accepted 9 December 2010; published 12 February 2011.

[1] This research examined hydrostatic groundwater model (MODFLOW) predictive adequacy and sensitivity in simulating hyporheic flow paths across a river step with a hydraulic jump. In a companion paper, we used flume and hydrodynamic model analysis to develop a refined conceptual model depicting these flow paths with zones of downwelling and upstream-directed flux below the step. The previous coarse conceptual model predicted uniform downstream-directed upwelling below the step. The hydrostatic model accurately predicted the downwelling and upstream-directed fluxes beneath the wave and jump but failed to predict the plunge pool downwelling, which is driven by dynamic pressures. Sensitivity tests varied riverbed topography and water surface profile geometry for a river with 1% slopes, 10 cm flow depths, and 50–150 cm long jets and jumps. The flow paths below the jet-jump region were driven by hydrostatic pressures and were highly sensitive to water surface profile and riverbed topography parameters. Failure to simulate the hydraulic jump caused errors in hyporheic flow path predictions beneath the jump region (~1 m long by ~0.5 m deep). If the jump was poorly parameterized, several meters of riverbed flow paths could be erroneously modeled as pointing upstream. The hyporheic zone may contain a spatial mosaic of aerobic and anaerobic waters regulating nutrient transformations and biologic productivity. Accurate parameterization of hydraulic jumps in hyporheic simulation has the potential to improve predictions and explain heterogeneous subsurface flow paths and associated nutrient patterns and ecosystem functions.

Citation: Endreny, T., L. Lautz, and D. Siegel (2011), Hyporheic flow path response to hydraulic jumps at river steps: Hydrostatic model simulations, *Water Resour. Res., 47*, W02518, doi:10.1029/2010WR010014.

1. Introduction

[2] In mountain rivers, the prevailing but coarse conceptual model for hyporheic exchange across a river step predicts downwelling flow paths upstream of the step and upwelling flow paths downstream of the step [see *Kasahara and Wondzell*, 2003, Figure 2; *Gooseff et al.*, 2006, Figures 2 and 3; *Harvey and Bencala*, 1993, Figure 10; *Tonina and Buffington*, 2009, Figure 6a; *Hester and Doyle*, 2008, Figure 2]. This prevailing model, referred to as the coarse conceptual model, has focused on the control exerted by the large elevation and associated pressure gradient across the step. The coarse conceptual model has not considered how hydraulic features associated with a step such as a plunging cascade and hydraulic jump influence the local flow paths and potentially disrupt the flow path directions. In a companion paper [*Endreny et al.*, 2011], we used flume and hydrodynamic model experiments to show how the plunging cascade and hydraulic jump downstream of the step significantly redirect hyporheic flow paths so that they deviate from the coarse conceptual model. We provide a refined conceptual model for hyporheic exchange across a river step in conditions of rapidly varied flow to resolve near-bed flow paths. Both conceptual models agree upstream of the step, but the refined model predicts downwelling downstream of the step, where the river plunges into the pool and beneath waves, and predicts upstream-directed upwelling along the longitudinal extent of the hydraulic jump. This paper examines how the hydrostatic model used in several of the above studies is capable of representing the refinements we have added to the conceptual model for hyporheic exchange at river steps.

1.1. Goal of Study

[3] The goal of this study is to examine how a standard hydrostatic groundwater model represents the hyporheic exchange flow paths across a step with rapidly varied flow including a hydraulic jump. Our first question is how well zones of downwelling and upstream-directed upwelling identified with the flume and hydrodynamic model are simulated by the hydrostatic model. Our second question is how sensitive these flow path predictions are to hydrostatic model parameterization of the water surface profile, step geology (e.g., shape and permeability), and riverbed topography. This research has the potential to identify and evaluate the significance of predictive errors in using a hydrostatic model

[1]Department of Environmental Resources Engineering, ESF, SUNY, Syracuse, New York, USA.
[2]Department of Earth Sciences, Syracuse University, Syracuse, New York, USA.

0043-1397/11/2010WR010014

when simulating hyporheic exchange at river steps with rapidly varied flow.

1.2. Models of Hyporheic Flow Paths and Hydraulics at a River Step

[4] The *Toth* [1963] conceptual model of flow patterns within an undulating hillslope section illustrates how hydrostatic pressure can drive local upslope-directed flow paths nested within a deeper set of uniform downslope-directed intermediate and regional flow paths. Unfortunately, the Toth conceptual model cannot simply be rotated to characterize flow patterns beneath the longitudinal section of a river step because the river boundary delivers hydrodynamic as well as hydrostatic pressures. Hyporheic flow paths most influenced by the step are relatively short and shallow local flow paths nearest the riverbed. The deeper intermediate flow paths are generally considered to move in a downriver direction beneath the riverbed. The downriver pressure gradient is the physical driver governing the advective component of hyporheic exchange across a river step [*Harvey and Bencala*, 1993; *Tonina and Buffington*, 2009]. Other components of hyporheic exchange that are potentially active across the step include diffusion, momentum, and sediment turnover [*Elliot and Brooks*, 1997; *Packman and Bencala*, 2000]. We isolate and focus on the advective component of exchange in this paper but recognize that these other exchange components (e.g., turbulent momentum transfer) are potentially sensitive to river hydraulics and could respond to cascade and hydraulic jump dynamics. In the advective component of exchange, the pressure gradient is the driving force. The pressure terms are represented in length units by velocity head, pressure head, and elevation head, which combine to equal hydraulic head.

[5] The refined conceptual model for hyporheic flow paths around a river step considers the river with rapidly varied flow. The river's rapidly varied flow may contain a nappe and jet passing over the step and farther downstream may contain a hydraulic jump with rollers and a wave (Figure 1a). A single sketch of rapidly varied flow creates a steady state representation of the dynamic river flow, which can contain aerated rollers and undulating waves [*Khatsuria*, 2004]. In the refined conceptual model (Figure 1a), the jet region contains supercritical flow (Froude number, $Fr_1 > 1$) with a flow depth y_1 and relatively high velocity. Immediately downstream of the jump is subcritical flow ($Fr_2 < 1$) with a flow depth y_2 and relatively low velocity. The refined conceptual model focuses on hyporheic flow paths downstream of the step. There is a small zone of upwelling along the face of the step as a result of surface water vortices and lower pressure head. There is downwelling beneath the nappe and wave (Figure 1a, white star) as well as upstream-directed upwelling beneath the longitudinal length of the hydraulic jump (Figure 1a, white rectangle). The upstream-directed subsurface flow paths and downstream-directed river flow connect to form a vertical eddy (Figure 1a, dashed oval). A simplified representation of this conceptual model removes the nappe and curvature from the water surface profile (Figure 1b). This simplified sketch represents output from a commonly used water surface profile model (Hydrologic Engineering Center's River Analysis System (HEC-RAS)) used later in this research. The uniform intermediate flow paths oriented as downstream-directed upwelling are beneath the heterogeneous local hyporheic flow paths.

[6] The coarse conceptual model (Figure 1c) illustrates a rapid drop across the step but no hydraulic jump. We leave the nappe out of this illustration because the coarse conceptual model did not consistently include the nappe and never explicitly modeled or discussed its effect on flow paths. The water surface curvature over the step is considered convex, and the curvature into the pool is considered concave [*Harvey and Wagner*, 2000]. Earlier studies of exchange across steps focused on the change in river water elevation across the step [*Gooseff et al.*, 2006; *Harvey and Bencala*, 1993; *Hester and Doyle*, 2008; *Kasahara and Wondzell*, 2003]. We identified two potential alternatives in the literature to this coarse conceptual model, but the ideas were not well developed. In a review paper, *Buffington and Tonina* [2009] hypothesized a local flow path of upstream-directed flux within a step-pool sequence (see their Figure 3b) with a sketch but did not discuss drivers of this vector or explain why it was absent in their sketch of exchange in cascade morphology. In a companion paper, *Tonina and Buffington* [2009] showed model output for a synthetic riffle-pool system with a hydraulic jump. In the porous matrix beneath this jump, they included vectors of upstream-directed upwelling but did not analyze or explain the flow paths. The research community has been developing an alternative to the coarse conceptual model, which is limited by its simplistic depiction of local hyporheic flow paths as uniform downstream-directed upwelling (Figure 1c).

[7] Studies generating flow paths conforming with the coarse conceptual model typically track only the deeper uniform flow paths and/or represent the river step with gradually varied flow. In gradually varied flow the flow depth generally follows the bed slope, changing with downstream distance but remaining either larger or smaller than the normal depth and not crossing the critical depth. While plunging cascades and hydraulic jumps are common to steps [*Wilcox and Wohl*, 2007], these earlier hyporheic modeling studies may not have identified rapidly varied flow features in their study sites or may have considered these features insignificant to their characterization of hyporheic exchange. Further, by employing hydrostatic models, these earlier studies accepted the tenet of the model as a simplification of the observed phenomenon [*Beven*, 1993; *Hassan*, 2004]. The hydrostatic model, by definition, neglects rapid changes in velocity head and stagnation pressure within a plunging cascade.

2. Methods

2.1. Comparison of Hydrodynamic and Hydrostatic Estimates of Hyporheic Paths

[8] In our companion paper [*Endreny et al.*, 2011] we demonstrated how the hydrodynamic model was capable of representing hyporheic exchange flow paths below a step by simulating dynamic and static pressures in the system. These pressure forces are represented as length terms by the elevation head, pressure head, and velocity head for each computational cell. In comparison, the hydrostatic model only simulates hydrostatic pressures and is represented by the piezometric head, which is the sum of the

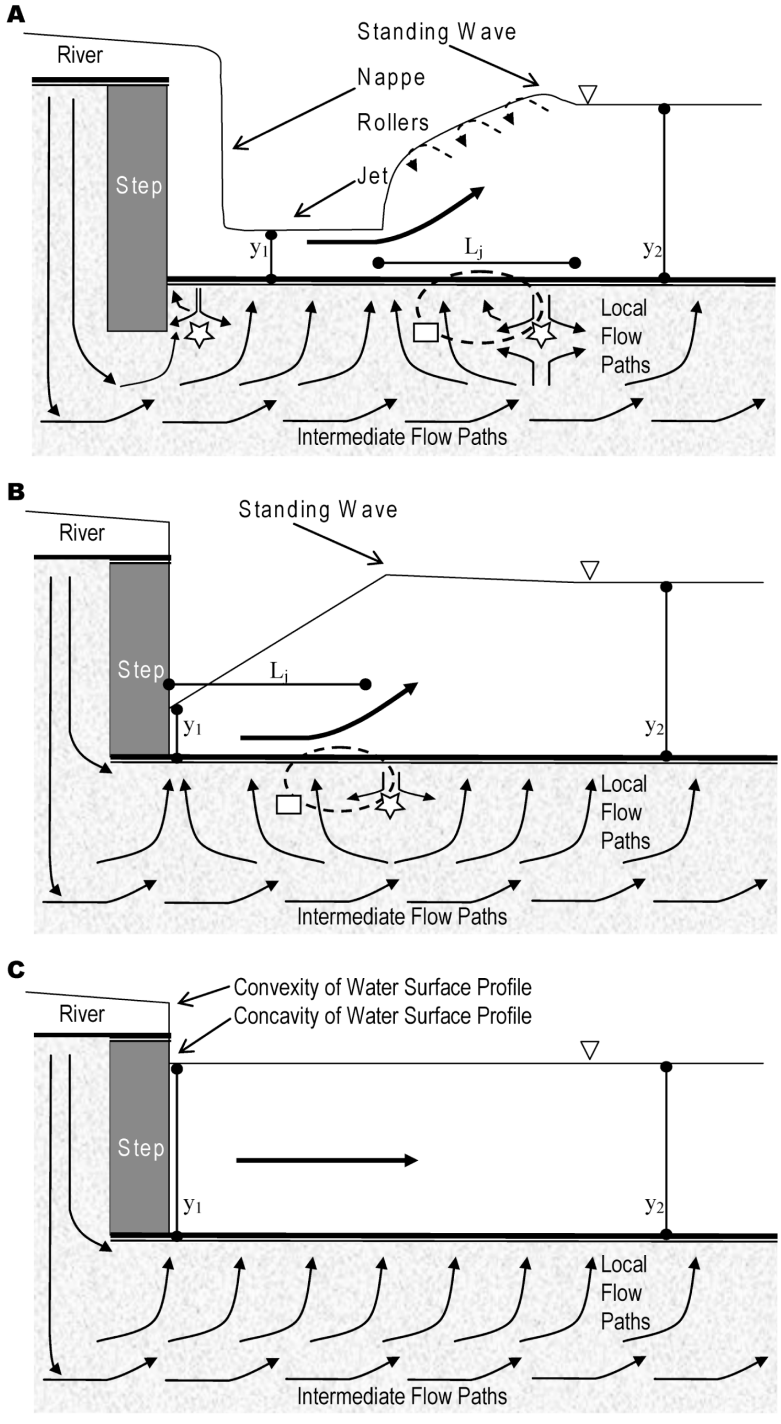

Figure 1. Sketch of water surface profile and hyporheic flow paths for (a) refined conceptual model with nappe across step, (b) refined conceptual model without nappe across step, and (c) coarse conceptual model without hydraulic jump.

elevation head and the pressure head generated by the height of water. The hydrodynamic model was the commercially available Flow3D, a 3-D computational fluid dynamic (CFD) model [*Flow Science*, 2009]. Flow3D simulates the open channel and porous media with an iterative finite difference–finite element approach to solve the pressure and velocity terms in the conservation of momentum and mass equations. The model's Navier-Stokes formulation of the momentum equation and use of the renormalized group two-equation $k-\varepsilon$ turbulence closure scheme are summarized in the companion paper [*Endreny et al.*, 2011], and all equations are given within the user manual [*Flow Science*, 2009]. The CFD model requires a river channel and riverbed simulation domain, upstream and downstream

boundary conditions of river stage, and adequate mesh resolution and parameter values to predict rapidly varied flow as well as hydraulic head (static and dynamic pressure forces) across the meshed domain. The free water surface elevation at each cell is obtained by having a water depth term in the momentum and mass conservation equations as they are simultaneously solved.

[9] The hydrostatic model used here was the U.S. Geological Survey supported 3-D MODFLOW groundwater water model [*Harbaugh*, 2005]. MODFLOW is a widely used analytical tool for hyporheic exchange research [*Gooseff et al.*, 2006; *Kasahara and Wondzell*, 2003; *Lautz and Siegel*, 2006; *Wondzell et al.*, 2009]. The riverbed domain is represented by 3-D cells, and each cell has a topographic elevation. Riverbeds are assigned an elevation and river stage, which combine to equal the piezometric head. This river stage is used to assign a head throughout the porous media. MODFLOW uses a finite difference approach to solve the conservation of mass and groundwater flow equation, and all governing equations are provided in the user manual [*Harbaugh*, 2005]. In MODFLOW runs we used the geometric multigrid solver and computed river conductance as a function of block-centered node spacing. The hydrodynamic and hydrostatic models represent porous media resistance differently. The hydrodynamic model uses drag coefficients to represent resistance in the Navier-Stokes momentum equation, while the hydrostatic model uses hydraulic conductivity to represent resistance in the Darcy-based groundwater flow equation.

[10] The hydrodynamic and hydrostatic models were parameterized to represent the flume experiments described in the companion paper [*Endreny et al.*, 2011]. The models simulated a 70 cm long by 7.5 cm wide channel with a 1% slope and 5 cm step, located 20 cm from the upstream boundary. Mesh resolution was 0.5 cm in the x, y, and z directions, taking a unit slice of the full channel width and prohibiting transverse exchange. The substrate had a porosity of 0.3 and extended 10 cm below the channel bed. The step was simulated as a solid block in the hydrodynamic model and as a no-flow boundary in the hydrostatic model. In each model the step spanned the entire drop and extended an additional 2 cm into the riverbed. The hydrodynamic model was sensitive to viscous forces and simulated water at 20°C. Drag coefficients were set to create an isotropic permeability of 3×10^{-5} cm^2 (equivalent hydraulic conductivity of 3 cm/s) to simulate flow resistance in a 1 cm median diameter gravel [*Bear*, 1988]. The hydrostatic model hydraulic conductivity was set to 3 cm/s. The hydrodynamic model used an upstream and downstream boundary condition of 4 cm deep water to simulate the water surface profile representing rapidly varied flow and the hydraulic jump. On the basis of a comparison with the flume-generated profile, this model-simulated water surface profile was considered a realistic representation of water depth along the channel. The free water surface elevation values calculated for each riverbed cell in the hydrodynamic model were used as the river boundary conditions for the equivalent cells in the hydrostatic model.

2.2. Hydrostatic Model Sensitivity to Representation of the Hydraulic Jump

[11] A sensitivity analysis of MODFLOW to the river boundary condition and hence the hydraulic jump is needed to identify opportunities and constraints on the use of MODFLOW in simulation of hyporheic exchange at river steps. Our methods followed those of *Hester and Doyle* [2008], who conducted an extensive sensitivity analysis of hyporheic exchange to river step height as well as geologic and hydrologic controls. Our study expands on theirs by adding the potential for MODFLOW to represent hyporheic flows paths beneath hydraulic jumps. We use the base case MODFLOW simulation of *Hester and Doyle* [2008] and the same 1-D HEC-RAS program [*U.S. Army Corps of Engineers* (*USACE*), 2008] in steady flow mode to generate the MODFLOW river boundary condition. The HEC-RAS program computes the water surface profile between cross sections using two alternative methods. In gradually varied flow, HEC-RAS solves the energy head form of the Bernoulli equation, accounting for friction losses, with an iterative standard step method [*USACE*, 2008]. Energy head includes channel elevation, water depth, and velocity head. Friction losses are represented along the channel perimeter with the Manning n roughness factor and at transitions with contraction and expansion coefficients. In rapidly varied flow, HEC-RAS solves a hydrostatic form of the momentum equation and mass conservation equation to estimate the water surface profile [*USACE*, 2008].

[12] We parameterized HEC-RAS to simulate a discharge of 0.2 m^3/s in a 30 m long by 3 m wide rectangular channel with a 1% longitudinal slope, a 0.03 Manning n roughness, 10 cm flow depths (y_2) for upstream and downstream boundary conditions, and the step top located at river station 15.1 m and the step base at river station 15.0 m. The HEC-RAS simulations used contraction and expansion coefficients of 0.6 and 0.8 for subcritical transitions and 0.05 and 0.1 for supercritical transitions and tolerances of 0.0003 m for the water surface and critical depth calculations [*USACE*, 2008]. Our MODFLOW simulation represented 5 m deep porous media with a porosity of 0.3 and hydraulic conductivity of 1.0×10^{-3} cm/s. MODFLOW was run in cross-section mode with a single row for the 3 m channel width and vertical layers of 5 cm thickness for each layer. The number of columns used to represent the 30 m river length varied in our sensitivity analysis, but for all simulations, MODFLOW cell centers (nodes) were located below HEC-RAS cross sections to precisely map the river boundary condition to the porous media mesh (Figure 2). In some simulations, smaller MODFLOW cells were placed between larger cells to represent rapid transitions in the water surface profile (identified in Figure 2 by arrows). In our sensitivity analysis, we generated 120 simulations by adjusting the following: HEC-RAS methods to estimate and MODFLOW node spacing to represent the hydraulic jump; MODFLOW node spacing and parameters to represent riverbed topography and step geology; step height (5, 20, 50, and 100 cm) in HEC-RAS and MODFLOW simulations; and node spacing (10, 20, 100, 300, and 500 cm) in cells not associated with the step or jump. Table 1 presents details on these parameter values for the sensitivity tests.

[13] HEC-RAS can estimate the water surface across a river step using three potential methods. We used these methods in this research. In comparing these three methods, consider a hydraulic jump to have fixed length L_j between y_1 and y_2, where L_j can be estimated by a Fr_1-sensitive jump equation [*Hager*, 1991]:

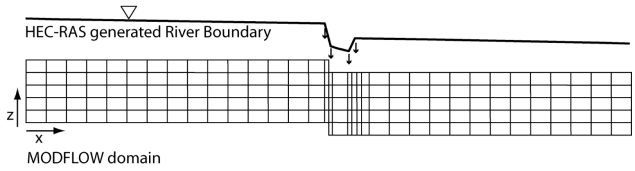

Figure 2. Hydrostatic groundwater model (MODFLOW) computational domain with water surface profile model (HEC-RAS) providing the boundary condition.

$$L_j = 6y_2, \quad Fr_1 > 4, \qquad L_j = 4y_2, \quad Fr_1 \sim 2. \tag{1}$$

[14] The first method is called no jump, and the user chooses to ignore rapidly varied flow and runs HEC-RAS in a fixed subcritical flow regime. In the no jump method, flow remains gradually varied, and there is no simulation of the hydraulic jump. In the second and third methods the user chooses to allow for rapidly varied flow and runs HEC-RAS in the mixed flow regime. The difference in these methods emerges with cross-section spacing. HEC-RAS will identify the cross sections and flow depths bounding a jump but does not establish a new cross section to terminate the hydraulic jump at L_j. HEC-RAS terminates the jump at the first cross section, where subcritical flow depth specific force is greater than supercritical flow depth specific force [*USACE*, 2008]. In the second method, called free jump, the user establishes cross sections free of any calculation of L_j that may cause a shorter or longer L_j than predicted by equation (1). In the third method, called set jump, the user establishes a set cross section to coincide with the L_j calculated with equation (1). In simulations involving hydraulic jumps, HEC-RAS engineers recommended use of the set jump or equivalent approach (C. Ackerman, personal communication, 2009). While the step ended at river station 15 m, the hydraulic jump often started farther downstream. The starting location was determined by the length of the supercritical jet L_{jet}, which started at the step base and extended to the start of the jump. We obtained the L_j values from equation (1) on the basis of determining $Fr_1 \sim 2$ for the 5 cm step and $Fr_1 > 4$ for the 20, 50, and 100 cm steps. For the 5 cm step, $L_j = 40$ cm, and for the 20 cm and higher steps, $L_j = 60$ cm. The L_j values were within 10% of the length predicted by the hydrodynamic model. The L_{jet} values were obtained from hydrodynamic simulation and parameterized in HEC-RAS by adjusting contraction and expansion coefficients.

[15] MODFLOW can simulate the step geology (e.g., permeability and shape) using two potential simulation methods. In contrasting these two methods, consider the step as an impermeable wooden board serving as an abrupt transition between the upstream and downstream sections of riverbed, where the step base is flush with the

Table 1. Parameters Adjusted in the HEC-RAS and MODFLOW Model Sensitivity Tests

Case	Hydraulic Jump	HEC-RAS Flow Regime	Step Geology/ Permeability	Step Start[a] (m)	Step End (m)	Sump Start (m)	Jump End[b] (m)	Step Height (cm)	Node Spacing[c] (cm)
1–5	Set jump	Mixed	Permeable	15.1–20	15	14.9	14.5	5	10, 20, 100, 300, 500
6–10	Set jump	Mixed	Permeable	15.1–20	15	14.8	14.2	20	10, 20, 100, 300, 500
11–15	Set jump	Mixed	Permeable	15.1–20	15	14.4	13.8	50	10, 20, 100, 300, 500
16–20	Set jump	Mixed	Permeable	15.1–20	15	14.3	13.7	100	10, 20, 100, 300, 500
21–24	Free jump	Mixed	Permeable	15.1	15	15	14.5–14.1	5, 20, 50, 100	10
25–28	Free jump	Mixed	Permeable	15.2	15	15	14.2–14	5, 20, 50, 100	20
29–32	Free jump	Mixed	Permeable	16	15	15	14	5, 20, 50, 100	100
33–36	Free jump	Mixed	Permeable	18	15	15	12	5, 20, 50, 100	300
37–40	Free jump	Mixed	Permeable	20	15	15	10	5, 20, 50, 100	500
41–44	No jump	Subcritical	Permeable	15.1	15	NA	NA	5, 20, 50, 100	10
45–48	No jump	Subcritical	Permeable	15.2	15	NA	NA	5, 20, 50, 100	20
49–52	No jump	Subcritical	Permeable	16	15	NA	NA	5, 20, 50, 100	100
53–56	No jump	Subcritical	Permeable	18	15	NA	NA	5, 20, 50, 100	300
57–60	No jump	Subcritical	Permeable	20	15	NA	NA	5, 20, 50, 100	500
61–65	Set jump	Mixed	Impermeable	15.1	15	14.9	14.5	5	10, 20, 100, 300, 500
66–70	Set jump	Mixed	Impermeable	15.1	15	14.8	14.2	20	10, 20, 100, 300, 500
71–75	Set jump	Mixed	Impermeable	15.1	15	14.4	13.8	50	10, 20, 100, 300, 500
76–80	Set jump	Mixed	Impermeable	15.1	15	14.3	13.7	100	10, 20, 100, 300, 500
81–84	Free jump	Mixed	Impermeable	15.1	15	15	14.5–14.1	5, 20, 50, 100	10
85–88	Free jump	Mixed	Impermeable	15.1	15	15	14.2–14	5, 20, 50, 100	20
89–92	Free jump	Mixed	Impermeable	15.1	15	15	14	5, 20, 50, 100	100
93–96	Free jump	Mixed	Impermeable	15.1	15	15	12	5, 20, 50, 100	300
97–100	Free jump	Mixed	Impermeable	15.1	15	15	10	5, 20, 50, 100	500
101–120	No jump	Subcritical	Impermeable	15.1	15	NA	NA	5, 20, 50, 100	10, 20, 100, 300, 500

[a]Permeable steps started one node spacing distance (either 10, 20, 100, 300, or 500 cm) upstream of 15 m, the step base.
[b]Free jump cases with 10–20 cm node spacing had jumps extend multiple cross sections, varying with jump height.
[c]Node spacing is HEC-RAS cross section and MODFLOW mesh spacing except at the step in impermeable simulations and the jump in set jump simulations.

downstream riverbed (see Figure 1b). The first method (permeable gradual step) represents the step as permeable with a gradual topographic transition between the upstream and downstream riverbed. The longitudinal transition between the step start (the top) and step end (the bottom) is arbitrarily set by the MODFLOW node spacing, regardless of HEC-RAS spacing. For a constant step height this method causes the step slope to decrease with increasing node spacing. This method was used by *Hester and Doyle* [2008] with a 3 m step transition distance. The transition is dependent on the node spacing, and with 10 cm node spacing, the step is equally abrupt to the second simulation method. The second method (impermeable abrupt step) represents the step as a no-flow impermeable boundary with an abrupt 10 cm topographic transition from step start to stop. This method more explicitly represents the river step geology. MODFLOW node spacing around the step changed with changes in hydraulic jump (no, free, or set jump). This represented model user approaches (i.e., if you simulate the set jump, you create additional MODFLOW nodes to capture the detailed river boundary condition) but did not comply with formal sensitivity tests that isolate a single changing parameter.

[16] After running the MODFLOW simulations, we used the MODPATH model [*Pollock*, 1994] to simulate particle advection in the riverbed. In all simulations a total of six particles were released upstream of the step. They were released 1 cm beneath the riverbed at river stations 15.5 m, 16 m, 16.5 m, 17 m, 17.5 m, and 18 m. For the MODFLOW simulations we noted areas downstream of the step where flow paths were upstream directed or downwelling. We also recorded the length of riverbed with upstream-directed hyporheic flux and the upstream-directed flux rate (m/s). For each MODPATH simulation we recorded the maximum depth that the particle traveled below the riverbed, the river station where the particle exited the hyporheic zone into the riverbed, and the particle flow path residence time in the riverbed.

3. Results and Discussion

3.1. Comparison of Hydrodynamic and Hydrostatic Estimates of Hyporheic Paths

[17] To compare flow paths between the hydrostatic and hydrodynamic modeling approaches, we assigned flow vectors from each cell into one of four flow path categories. These flow path categories are relative to the orientation of the river flow and riverbed. The flow directions are as follows: downstream-directed downwelling, where vectors are oriented downstream and away from the riverbed; downstream-directed upwelling, where vectors are oriented downstream and toward the riverbed; upstream-directed downwelling, where vectors are oriented upstream and away from the riverbed; and upstream-directed upwelling, where vectors are oriented upstream and toward the riverbed. Below the step the coarse conceptual model for hyporheic exchange flow paths predicts uniform downstream-directed upwelling. The refined conceptual model predicts areas in all four categories, and the hydrodynamic simulation output is considered representative of this refined conceptual model. In the top 4 cm of riverbed, 87% of hydrodynamic cells and 83% of hydrostatic cells were not downstream-directed upwelling. The two models were within 3% agreement for the number of cells estimated in each flow direction.

[18] The best agreement between hydrodynamic and hydrostatic hyporheic flow paths was beneath the jump and its wave, where piezometric head was the dominant driver (Figure 3). Immediately upstream of the step a 1 cm^2 area of streambed in both models experienced upwelling and did not comply with the coarse conceptual model. This area of departure is not considered further in this research. Downstream of the step the section of best agreement begins with the start of the jump and continues downriver (Figure 3, dashed rectangle). The longitudinal midpoint of this zone is where the water surface profile has a local maximum elevation and vectors are close to vertically downward. This local maximum elevation is called the wave, and its water surface profile regulates hyporheic flow vectors near the riverbed. Flow vectors upstream of the wave are oriented as upstream directed, while those downstream of the wave are downstream directed; with depth they transition from downwelling to upwelling. Beneath the wave in the lower porous layers, there remained a strong agreement between the hydrodynamic and hydrostatic flow paths, with each ending the downwelling signal between 4 and 5 cm below the riverbed.

[19] The biggest differences between the hydrodynamic and hydrostatic hyporheic flow paths were beneath the nappe, where dynamic pressures were active, and beneath the jet, where stagnation pressures were active (Figure 3, see labels). Vortices in the nappe lowered the riverbed pressures and initiated a region of upwelling along the base of the step. This is evident in the first three flow vectors downstream of the step (Figure 3a, black circle). Two of these flow vectors have an upstream-directed upwelling orientation. In contrast, the hydrostatic model predicted downwelling at the base of the step as a result of the nappe profile generating locally high piezometric head. The stagnation pressure at the nappe-jet transition in the hydrodynamic simulation caused downwelling, which is evident in the fourth, fifth, and sixth flow vectors after the step (Figure 3a, white circle). In contrast, the hydrostatic model predicted upwelling in this same zone, caused by low piezometric head in the supercritical jet.

[20] Hydrostatic model flow paths below the step did not perfectly match the hydrodynamic model predictions and departed from the refined conceptual model of flow paths. However, the hydrostatic model predictions were more closely aligned with the refined than the coarse conceptual model. The hydrostatic model flow paths were in all four orientations and did not comply with the uniform downstream-directed upwelling pattern predicted by the coarse conceptual model. The two major areas of error in the hydrostatic model predictions were in the nappe and the nappe transition to the jet. This error occurred within a 5 cm longitudinal length of riverbed nearly equivalent to the flow depth. Given this length is 75% smaller than the length of the agreement zone, we accepted the hydrostatic model, when parameterized with a hydraulic jump and fine grid spacing, as mostly representative of the refined conceptual model. As we show in section 3.2, this nappe zone of erroneous prediction is not always a prominent zone. It is neglected by the HEC-RAS simulations used to estimate

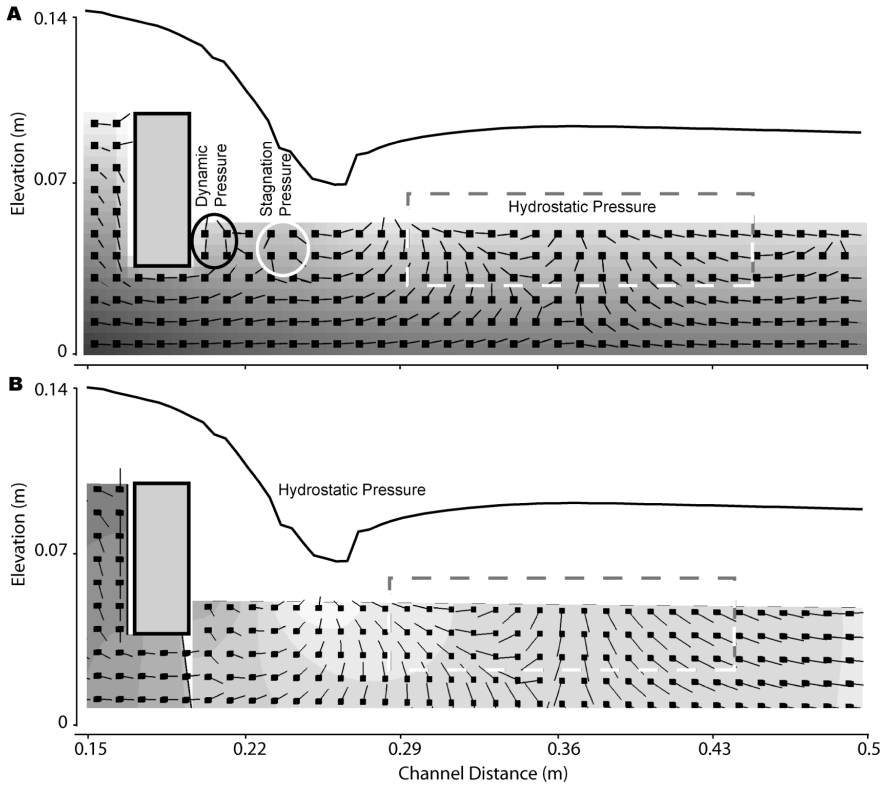

Figure 3. Flow path vectors from the (a) hydrodynamic model (Flow3D) and (b) hydrostatic model (MODFLOW). Both models used the same water surface profile, but Flow3D simulated dynamic and static pressures. The porous media gray scale contours the pressure head (darker grays are higher pressures). The flow vectors are shown for every other cell and spaced at 1 cm. The shaded rectangle is the flow origin, and the black line shows the flow direction.

the water surface profile across the step. HEC-RAS treats the nappe with zero thickness (see Figure 1b and Figure 2). We explain the reason for this in section 3.2.

3.2. Hydrostatic Model Sensitivity to Representation of the Hydraulic Jump

[21] To characterize the hyporheic flow paths from the 120 sensitivity analysis simulations, we provide statistical summaries supplemented with a few illustrations of the simulated flow paths. The statistical summaries are box-and-whisker plots comparing model output metrics by step height, step geology/permeability, and jump simulation method (Figure 4). When interpreting these box-and-whisker plots, we used the set jump output as a base standard. We selected the set jump as the standard because its water surface profile most closely matched the flume and hydrodynamic profiles [*Endreny et al.*, 2011]. Illustrations of water surface profiles and flow paths are provided for some simulations with a 5 cm high step to help visualize the different water surface profiles and step geometries as a function of node spacing. The three water surface profiles are shown for the permeable gradual step with 300 cm node spacing (Figure 5), the impermeable abrupt step with 300 cm node spacing (Figure 6), and the impermeable abrupt step with 20 cm node spacing (Figure 7). The top profile in Figures 5–7 is the no jump method, the middle profile is the free jump method, and the bottom profile is the set jump method. The flow path vectors only report flow direction and do not represent differences in flux rates. Black rectangles were placed around groups of flow vectors to highlight differences within and between the separate jump methods. White stars mark areas with reversed hyporheic circulation cells.

[22] The HEC-RAS water surface profile did not represent the nappe region simulated by the hydrodynamic model, but it could represent features of the hydraulic jump. The lack of a simulated nappe above the downstream riverbed occurs as a result of the absence in HEC-RAS of a computational domain along the face of the step. In contrast, the hydrodynamic model had a computational mesh along the step face and occupied those nodes with the nappe. The HEC-RAS water surface profiles varied substantially between the three jump simulation methods (no jump, free jump, and set jump; compare the profiles in Figures 5, 6, or 7) and also varied within a single method as a result of step geometry (see Figure 5a versus Figure 6a or Figure 5b versus Figure 6b) and riverbed node spacing (see Figure 6b versus Figure 7b or Figure 6c versus Figure 7c).

[23] Maximum path depth, as indicated by particle tracking, increased with step height regardless of the jump and step simulation method (Figures 4a and 4b), and deeper paths were associated with particles released farther upstream of the step. As node spacing decreased, the particles released closest to the step had deeper paths, but otherwise, there was

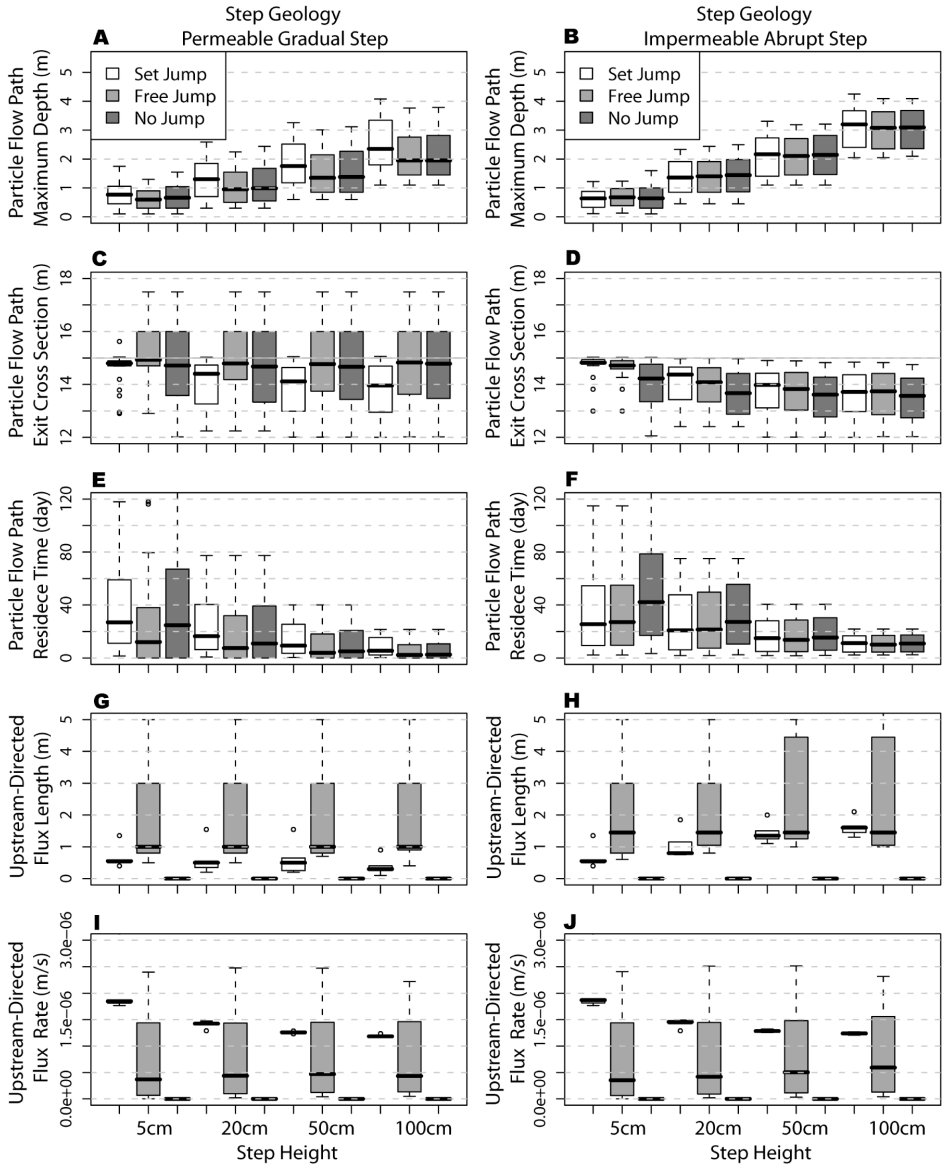

Figure 4. Sensitivity analysis results for hydrostatic model (MODFLOW) and particle-tracking simulations. Simulation results (left) with a permeable gradual step and (right) with an impermeable abrupt step are shown. Results are compared by jump simulation (set jump, free jump, and no jump) and step height (5, 20, 50, and 100 cm). Each box unit contains output from five node spacings (10, 20, 100, 300, and 500 cm), and for path output each node spacing has output from six particles. Box plots report (a, b) particle flow path maximum depth, (c, d) particle flow path exit cross section, (e, f) particle flow path residence time, (g, h) upstream-directed flux length, and (i, j) upstream-directed flux rate.

little impact to path depth from model node spacing. For simulations with impermeable abrupt steps the set jump, free jump, and no jump flow paths had equivalent maximum depths. When simulations were changed to permeable gradual steps, all flow paths became shallower, but set jump paths changed the least. This is explained by the set jump simulation maintaining a consistent water surface profile with changing step geologies. For the permeable and impermeable simulations, additional 10 cm long MODFLOW cells were established at the top and bottom of the step to maintain the jet and jump lengths (see Figures 5c and 6c). As a consequence, the set jump profiles had stronger pressure gradients (see Figures 5c versus 5b and 5c versus 5a) and deeper flow paths.

[24] Particles exited the hyporheic zone at different riverbed locations as a result of changes in jump simulation and step parameterization methods (separate tests showed exit location was insensitive to MODFLOW node spacing alone). For permeable steps the set jump water surface profile caused the distribution of particles to exit the hyporheic zone farther downstream (lower cross section values) than the other jump simulations with permeable steps (Figure 4c). As step height increased, the set jump distribution of particles (25th, 50th, and 75th percentiles) traveled farther

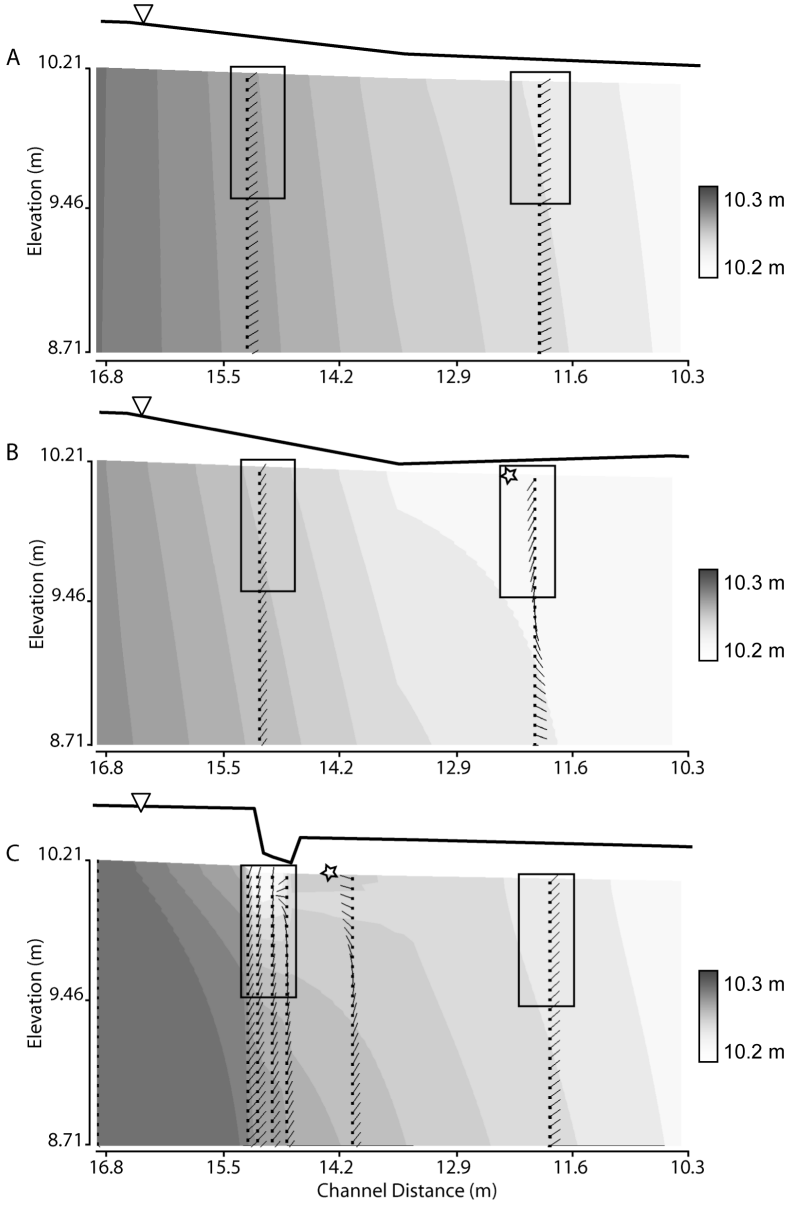

Figure 5. Simulation output for 5 cm step with 300 cm node spacing and permeable gradual step (cases 53, 33, and 4 in Table 1). Output is a longitudinal section view of the hydrostatic model (MODFLOW) pressure gradient contour (gray scale, darker is higher pressure) and flow path vectors (square is center of cell) for water surface profiles with (a) no jump, (b) free jump, and (c) set jump. Rectangles highlight flow vectors to compare within and between water surface profiles. Stars indicate reversed hyporheic circulation cells.

downstream. The particle released closest to the step exited at the base of the step (15 m cross section). This upwelling at the base of the step occurred because of the lack of nappe in the HEC-RAS water surface profile. Approximately half of the free jump and no jump particles exited along the face of the permeable step upstream of the 15 m cross section. For the impermeable step simulations the particles from all three jump methods exited the hyporheic zone downstream of the step (Figure 4d). Particles associated with the no jump simulation exited the hyporheic zone further downstream than particles with the set jump and free jump simulations. This was due to the supercritical flow region in the set jump and free jump simulations causing a local minimum pressure (see Figures 7b and 7c) that directed the flow paths into the river. As step height increased, the difference between set jump and free jump exit locations diminished because their equivalent pressure gradient across the step governed flow more than the small pressure gradient differences within the jump.

[25] Particle flow path residence times decreased with step height (Figures 4e and 4f). With permeable steps (Figure 4e) the set jump simulations had some of the longest residence times because of their deeper and longer flow paths. As a result of weaker piezometric head gradients in

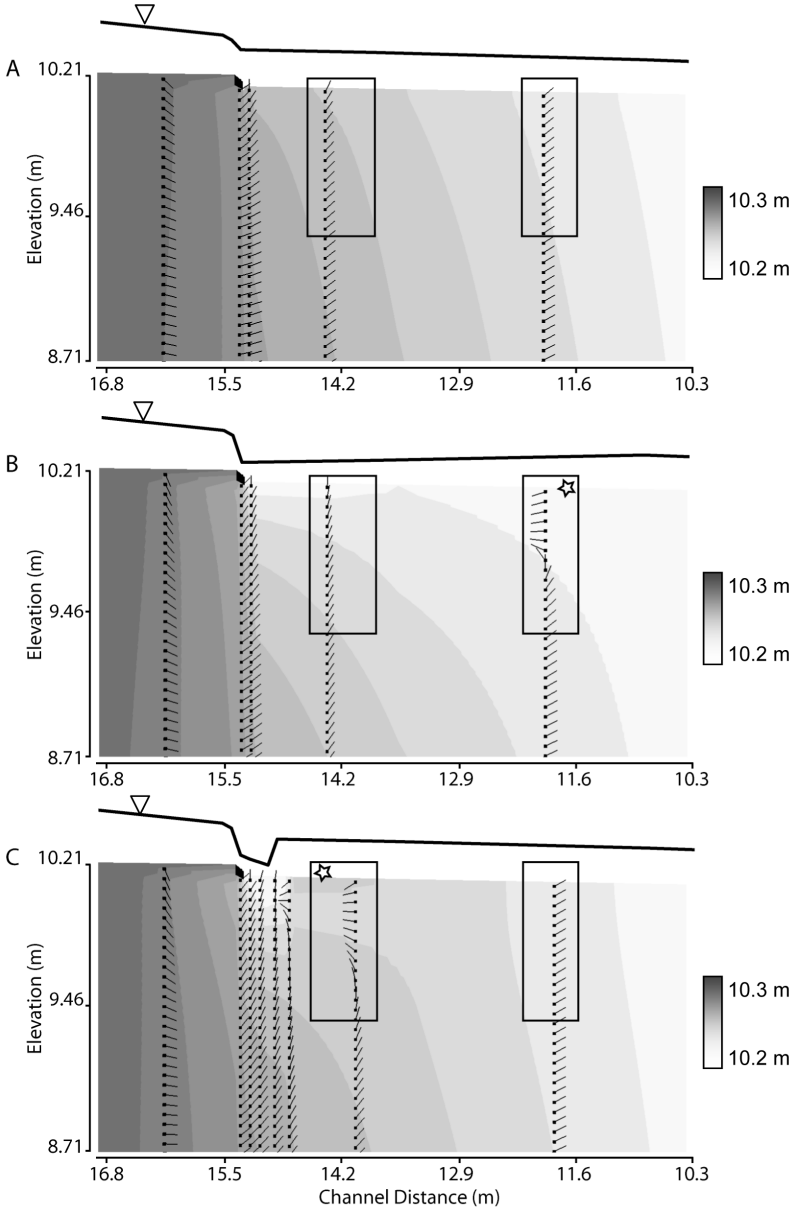

Figure 6. Simulation output for 5 cm step with 300 cm node spacing and impermeable abrupt step (cases 113, 93, and 64 in Table 1). Output is a longitudinal section view of the hydrostatic model (MODFLOW) pressure gradient contour (gray scale, darker is higher pressure) and flow path vectors (square is center of cell) for water surface profiles with (a) no jump, (b) free jump, and (c) set jump. Rectangles highlight flow vectors to compare within and between water surface profiles. Stars indicate reversed hyporheic circulation cells.

the no jump simulations the no jump and set jump residence times were comparable despite the shallower paths of the no jump particles. In contrast, the free jump simulations had some of the shortest times because of shallow paths and relatively strong pressure gradients. With impermeable steps (Figure 4f) the flow path residence times for the set jump and free jump simulations were similar and lower than flow path residence times for the no jump scenario. Particles in the simulations with a jump had shorter flow path residence times and distances as a result of high flux rates of upwelling within the supercritical jet.

[26] The upstream-directed flow paths varied between the three methods for simulating the hydraulic jump. We compared predictions of upstream-directed flow paths by comparing the total length of riverbed cells with this flux direction (Figures 4g and 4h) and comparing flux rates in those cells (Figures 4i and 4j). The no jump simulations had 0 cm length of upstream-directed flux. The free jump simulations had greater upstream-directed flux lengths than set jump simulated lengths, where free jump lengths extended the length of the node spacing. The upstream-directed lengths were relatively insensitive to step height

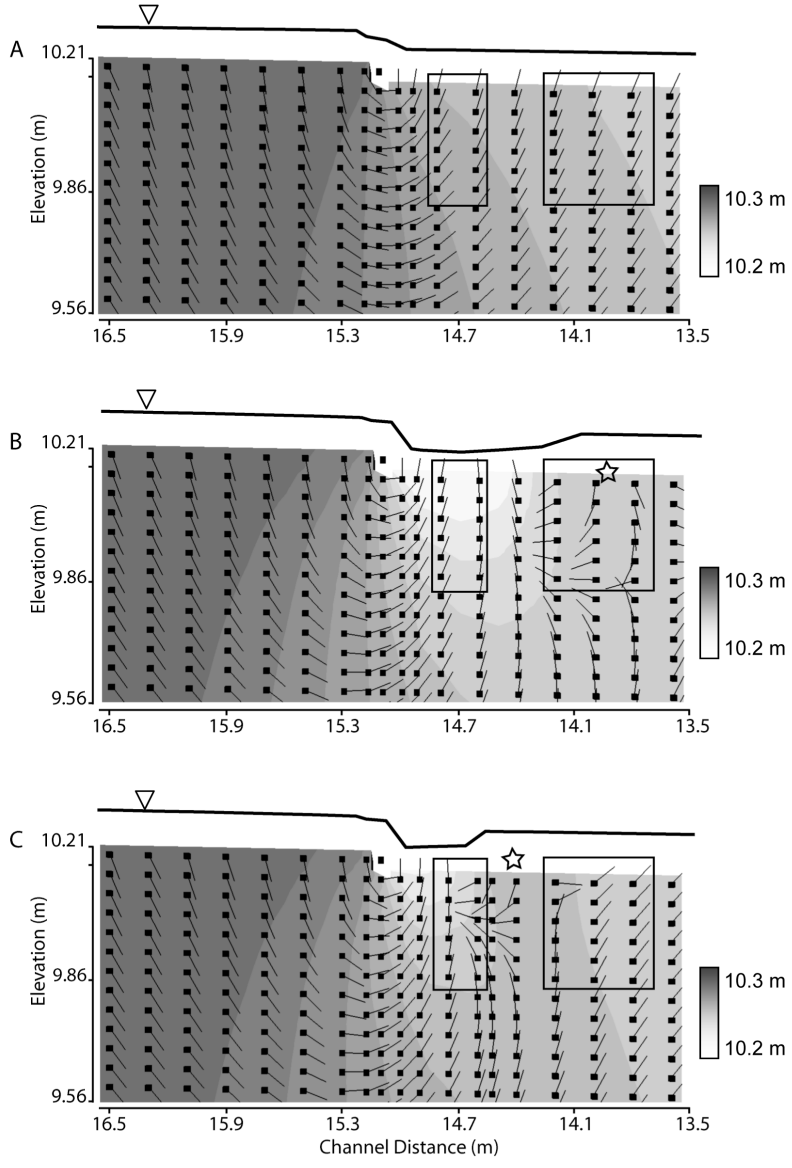

Figure 7. Simulation output for 5 cm step with 20 cm node spacing and impermeable abrupt step (cases 105, 85, and 45 in Table 1). Output is a longitudinal section view of the hydrostatic model (MODFLOW) pressure gradient contour (gray scale, darker is higher pressure) and flow path vectors (square is center of cell) for water surface profiles with (a) no jump, (b) free jump, and (c) set jump. Rectangles highlight flow vectors to compare within and between water surface profiles. Stars indicate reversed hyporheic circulation cells.

for permeable step simulations. In contrast, in impermeable step simulations, the upstream-directed flux lengths increased with step height (Figure 4h). The length of upstream-directed flux corresponded to the combined L_{jet} and L_j and had median lengths between 0.50 and 1.3 m for the set jump. The upstream-directed flux reached riverbed depths of 30–60 cm, with the horizontal extent diminishing with depth. While the free jump had greater lengths of upstream-directed flux, it had significantly weaker median flux rates than the set jump rates for both step geometries (Figures 4i and 4j). For set jump simulations the upstream-directed flux rate tended to decrease with step height because of stronger downstream-directed fluxes beneath the higher steps. The free jump's larger upstream-directed flux rates were for simulations using 10 and 20 cm node spacing. These flux rates did not vary with step height, and the distribution of rates greatly overestimated and underestimated the set jump flux rates.

[27] Vertical downwelling flow paths downstream of the step were absent in all of the no jump simulations. Downwelling flow paths were present in free jump and set jump simulations at all node spacings for the 5 and 20 cm steps. For the 50 and 100 cm step heights, only the 10 cm node spacing consistently simulated downwelling, and it was otherwise absent. This was because the 10 cm node forced an abrupt pressure gradient along the jump to counter the strong upwelling pressure gradients across the step. When downwelling was present downstream of the step, the flux

extended into the first four vertical model layers, between 5 and 20 cm deep. If model layering was changed from 5 to 25 cm, this downwelling flux was not consistently predicted. The longitudinal extent of downwelling typically ranged from 10 to 40 cm along the riverbed. In set jump simulations of 5 and 20 cm steps with node spacing equal to or greater than 100 cm, the downwelling flux was only present in the smaller cells (10–20 cm) bracketing the jump. In free jump simulations of 5 cm steps the downwelling flux could extend longitudinally along several meters of riverbed. Its length beneath the jump was limited by the length of the node spacing. As a result, free jump simulations could predict 100, 300, or 500 cm downwelling lengths when the set jump predicted less than 50 cm of downwelling.

[28] Our sensitivity analysis results generally agree with the key findings of *Hester and Doyle* [2008]. They reported trends of increasing particle flow depths, flow lengths, and decreasing residence times when step height was increased from 5 to 100 cm. Our results show how these trends move at different rates depending on model parameterization of the hydraulic jump, river step, and node spacing. Shorter node spacings with free jump simulations agreed better with the set jump simulations. Set jump simulations had greater flow path depths, lengths, and residence times than the free jump and no jump simulations when we used the permeable step approach of *Hester and Doyle* [2008]. When we simulated the impermeable abrupt step, the set jump flow path depths, lengths, and residence times were comparable to free jump estimates. Upstream-directed flow paths and downwelling flow paths beneath the step were highly sensitive to model parameterization, and estimates of these fluxes with the free jump and no jump methods compare poorly with the set jump estimates.

3.3. Operational Models for Hyporheic Flow Paths in Rapidly Varied Flow

[29] Our research focused on hyporheic flow path heterogeneities beneath river steps, but we suspect flow path heterogeneities are also established by rapidly varied flow in other coastal and fluvial systems, such as shoreline waves or river riffles. Although our observed and modeled flow path heterogeneities have limited spatial extent, their presence in nature might explain heterogeneities in ecosystem structure and function. As an example, ecologists have identified how the hyporheic zone sustains biologic productivity in the river channel by critically regulating nutrient fate and transport [*Stanford and Ward*, 1988]. While nutrient transformation, such as nitrification in oxygen-rich zones and denitrification in oxygen-depleted zones, is known to have spatial complexity [*Triska et al.*, 1993], the spatial patterns are not explained by the coarse conceptual model of uniform downwelling and upwelling [*Lautz and Fanelli*, 2008]. The flow path heterogeneities beneath spatially complex channel flows could help explain these patterns. A field or model observation of river dynamics may trigger use of the refined conceptual model to help explain hyporheic flows, spatial patterns of nutrient transformation, and the biological communities connected to these nutrients. To further examine the extent and influence of these heterogeneous flow paths in the hyporheic zone, the scientific community needs conceptual and operational models. Our study has shown that the hydrodynamic model provides a better representation than the hydrostatic model of hyporheic flow path heterogeneity beneath the river step with rapidly varied flow. However, the hydrostatic model was capable of matching nearly 80% of the hydrodynamic model predicted flow path heterogeneity when parameterized with a detailed and accurate water surface profile.

[30] A key benefit of using a hydrodynamic model for a coupled river-aquifer system is seamless simulation of the velocity profile, water surface profile, and the associated dynamic and static pressure heads. After a review of hyporheic literature we only identified two research groups publishing hydrodynamic simulations [*Cardenas and Wilson*, 2007; *Crispell and Endreny*, 2009]. For certain hyporheic study scales and analyses the HEC-RAS and MODFLOW hydrostatic model approach is certainly adequate, and while the hydrodynamic model is more flexible, it has greater relative complexity and cost. The hydrostatic model is a more widely available and utilized modeling tool. Its simulation errors of the hyporheic exchange beneath rapidly varied flow might be corrected by amplifying or muffling river stage and hence hydrostatic head to represent dynamic pressure forces. Two areas where this is needed at the river step are for the nappe and jet regions. Below the nappe, where vortices lower the pressure head, the hydrostatic model could be given a local minimum water surface to induce upwelling. Below the nappe-jet transition, where stagnation pressures increase static pressure head, the hydrostatic model could use a local maximum water surface to generate downwelling. If these regions are important in the simulation, it may be more accurate and simple to simulate the system with a hydrodynamic model. The much longer section of riverbed beneath the hydraulic jump is accurately modeled by the hydrostatic model.

4. Conclusions

[31] Hydrostatic model simulation of hyporheic exchange around a river step was capable of representing nearly 80% of the streambed flow path heterogeneity predicted by a hydrodynamic model. The hydrostatic model failed to represent the dynamic pressure forces associated with the vortices in the nappe and stagnation in the jet. This caused the model to erroneously omit upwelling zones caused by the vortices and downwelling caused by the stagnation. The hydrostatic model predictions were most representative when the water surface profile boundary condition and riverbed topography explicitly represented the observed conditions. When the hydraulic jump was not represented in the model boundary condition, the hyporheic flow paths had a uniform pattern of downstream-directed upwelling. When the jump was represented, these uniform flow paths were replaced by a heterogeneous pattern of flows including downwelling fluxes and upstream-directed fluxes. These heterogeneous flows had a longitudinal extent equal to the jet and jump lengths, ranging from 40 to 130 cm, and reached depths between 5 and 60 cm into the riverbed. When the hydraulic jump was erroneously extended as a result of arbitrary model node spacing, these upstream-directed flow lengths had overestimated lengths and underestimated flux rates. If the river step was simulated as an impermeable abrupt riverbed transition, the upstream-directed fluxes had greater longitudinal extent and vertical

depth than when the step was simulated as permeable and gently sloped. These flow path heterogeneities significantly impacted hyporheic residence times. Surrounding these downwelling and upstream-directed upwelling fluxes were deeper intermediate flow paths traveling downstream. As the intermediate flow upwelled toward the riverbed, it would experience flow reversals beneath the jump. River water downwelling into this same riverbed zone beneath the jump travels back upstream along the upstream-directed flow paths and generates what we call reversed hyporheic circulation cells. We expect these flow path heterogeneities to reside beneath other fluvial and coastal environments with rapidly varied flow, and we encourage further investigation into their physical nature and their impacts on ecosystem structure and function.

[32] **Acknowledgments.** This research was funded by the National Science Foundation EAR under grant 0450317 and CBET SGER under grant 0836354. The authors thank M. Gooseff and E. Hester for sharing details of their modeling analysis, R. Winston of the U.S. Geological Survey for assistance with MODFLOW, and C. Ackerman of the U.S. Army Corps of Engineers for assistance with HEC-RAS. Editorial guidance from E. Wohl and comments from E. Hester and two anonymous reviewers were extremely useful in manuscript revisions.

References

Bear, J. (1988), *Dynamics of Fluids in Porous Media*, 764 pp., Dover, Mineola, N. Y.

Beven, K. (1993), Prophecy, reality, and uncertainty in distributed hydrological modeling, *Water Resour.*, *16*, 41–51.

Buffington, J. M., and D. Tonina (2009), Hyporheic exchange in mountain rivers II: Effects of channel morphology on mechanics, scales, and rates of exchange, *Geogr. Compass*, *3*, 1–25, doi:10.1111/j.1749-8198.2009.00225.x.

Cardenas, M. B., and J. L. Wilson (2007), Hydrodynamics of coupled flow above and below a sediment-water interface with triangular bedforms, *Adv. Water Resour.*, *30*(3), 301–313.

Crispell, J. K., and T. A. Endreny (2009), Hyporheic exchange flow around constructed in-channel structures and implications for restoration design, *Hydrol. Processes*, *23*(8), 1158–1168.

Elliot, A. H., and N. H. Brooks (1997), Transfer of nonsorbing solutes to a streambed with bed forms: Laboratory experiments, *Water Resour. Res.*, *33*(1), 137–151.

Endreny, T., L. Lautz, and D. Siegel (2011), Hyporheic flow path response to hydraulic jumps at river steps: Flume and hydrodynamic models, *Water Resour. Res.*, W02517, doi:10.1029/2009WR008631.

Flow Science (2009), FLOW 3D version 9.4, user's manual, 641 pp, Sante Fe, N. M.

Gooseff, M. N., J. K. Anderson, S. M. Wondzell, J. LaNier, and R. Haggerty (2006), A modeling study of hyporheic exchange pattern and the sequence, size and spacing of stream bedforms in mountain stream networks, Oregon, USA, *Hydrol. Processes*, *20*(11), 2443–2457.

Hager, W. H. (1991), *Energy Dissipators and Hydraulic Jump*, Kluwer Acad., Dordrecht, Netherlands.

Harbaugh, A. W. (2005), MODFLOW-2005, the U.S. Geological Survey modular ground-water model—The ground-water flow process, *U.S. Geol. Surv. Tech. Methods*, *6-A16*, 253 pp.

Harvey, J. W., and K. E. Bencala (1993), The effect of streambed topography on surface-subsurface water exchange in mountain catchments, *Water Resour. Res.*, *29*(1), 89–98.

Harvey, J. W., and B. J. Wagner (2000), Quantifying hydrologic interactions between streams and their subsurface hyporheic zones, in *Streams and Ground Waters*, edited by J. B. Jones and P. J. Mulholland, pp. 3–44, Elsevier, San Diego, Calif.

Hassan, A. E. (2004), Validation of numerical ground water models used to guide decision making, *Ground Water*, *42*(2), 277–290.

Hester, E. T., and M. W. Doyle (2008), In-stream geomorphic structures as drivers of hyporheic exchange, *Water Resour. Res.*, *44*, W03417, doi:10.1029/2006WR005810.

Kasahara, T., and S. M. Wondzell (2003), Geomorphic controls on hyporheic exchange flow in mountain streams, *Water Resour. Res.*, *39*(1), 1005, doi:10.1029/2002WR001386.

Khatsuria, R. M. (2004), *Hydraulics of Spillways and Energy Dissipators*, CRC Press, Boca Raton, Fla.

Lautz, L. K., and R. M. Fanelli (2008), Seasonal biogeochemical hotspots in the streambed around restoration structures, *Biogeochemistry*, *91*(5), 85–104.

Lautz, L. K., and D. I. Siegel (2006), Modeling surface and ground water mixing in the Hyporheic Zone using MODFLOW and MT3D, *Adv. in Water Resour.*, *29*(11), 1618–1633.

Packman, A. I., and K. E. Bencala (2000), Modeling surface-subsurface hydrologic interactions, in *Streams and Ground Waters*, edited by J. B. Jones and P. J. Mulholland, pp. 45–80, Elsevier, San Diego, Calif.

Pollock, D. W. (1994), User's guide for MODPATH/MODPATH-PLOT, version 3: A particle tracking post-processing package for MODFLOW, the U.S. Geological Survey finite-difference ground-water flow model, *U.S. Geol. Surv. Open File Rep.*, *94-464*.

Stanford, J. A., and J. V. Ward (1988), The hyporheic habitat of river ecosystems, *Nature*, *335*(6185), 64–66.

Tonina, D., and J. M. Buffington (2009), Hyporheic exchange in mountain rivers I: Mechanics and environmental effects, *Geogr. Compass*, *3*, 1–24, doi:10.1111/j.1749-8198.2009.00226.x.

Toth, J. (1963), A theoretical analysis of groundwater flow in small drainage basins, *J. Geophys. Res.*, *68*(16), 4795–4812.

Triska, F. J., J. H. Duff, and R. J. Avanzino (1993), The role of water exchange between a stream channel and its hyporheic zone in nitrogen cycling at the terrestrial aquatic interface, *Hydrobiologia*, *251*(1-3), 167–184.

U.S. Army Corps of Engineers (USACE) (2008), HEC-RAS River Analysis System hydraulic reference manual version 4.0, *Rep. CPD-68*, Hydrol. Eng. Cent., Davis, Calif.

Wilcox, A. C., and E. E. Wohl (2007), Field measurements of three-dimensional hydraulics in a step-pool channel, *Geomorphology*, *83*(3-4), 215–231.

Wondzell, S. M., J. LaNier, and R. Haggerty (2009), Evaluation of alternative groundwater flow models for simulating hyporheic exchange in a small mountain stream, *J. Hydrol.*, *364*(1-2), 142–151.

T. Endreny, Department of Environmental Resources Engineering, 423 Baker Lab, ESF, SUNY, Syracuse, NY 13210, USA. (te@esf.edu)

L. Lautz, Department of Earth Sciences, 204 Heroy Geology Lab, Syracuse University, Syracuse, NY 13210, USA. (lklautz@syr.edu)

D. Siegel, Department of Earth Sciences, 307 Heroy Geology Lab, Syracuse University, Syracuse, NY 13210, USA. (disiegel@syr.edu)